Asociación Argentina
de Mecánica Computacional

Mecánica Computacional Vol XLII, pp. 505-514
A. Caggiano, G. Etse, P. Folino, M. Goldschmit, M. Pucheta, M. Storti (Eds.)
V. Cortínez, J. Inaudi, O. Moller (Issue eds.)
Buenos Aires, November 11-14, 2025

# DEVELOPMENT OF 2D COMPUTATIONAL MODELS FOR THE ESTIMATION OF FREIGHT VEHICLE-INDUCED VIBRATIONS ON HETEROGENEOUS ROADWAY STRUCTURES

**José A. Inaudi**[a,b] **and Ignacio Canigia**[b,c]

[a]*Facultad de Ingeniería, Universidad Católica de Córdoba , Córdoba, Argentina,*
*https://www.ucc.edu.ar/ingenieria*

[b]*Facultad de Ciencias Exactas Físicas y Naturales, Universidad Nacional de Córdoba, Argentina,*
*jose.antonio.inaudi@unc.edu.ar, icanigia@unc.edu.ar https://fcefyn.unc.edu.ar/*

[c]*IDIT-CONICET-Universidad Nacional de Córdoba, Córdoba, Argentina.*

**Keywords:** Trains, Vibrations, Fourier.

**Abstract.** The interaction between vehicles moving on a continuous elastic medium and underlying support layers generates induced vibrations that may affect surrounding structures. In environmental impact studies for proposed and planned new railway lines, it is frequently necessary to characterize vibration intensities for different track support structural packages. For train systems, in addition to the mechanical properties of the foundation package, both rail roughness and wheel roughness (flat-wheel conditions) become particularly relevant. This work develops a modeling approach for parametric analysis of such systems, employing a matrix assembly methodology in generalized coordinates along with global interpolation functions for the rail (modeled as a constant-section Euler-Bernoulli beam) and discrete coordinates to represent sleeper kinematics and elastic support medium deformation. Rail deformation is approximated through superposition of a Fourier basis with interpolation functions accounting for rigid body displacements of the rail. The implementation of global interpolation functions and the orthogonality properties of the rail deformation interpolation functions enable efficient assembly of the system's motion equations matrices (some being time-variant) for the coupled vehicle-track model incorporating rail, sleepers, and elastic foundation support. Through numerical integration of the linear time-variant model, rail vibrations are analyzed under the assumption of rigid wheel-rail contact. Results from this primary model are compared with a mass-mass coupling model using a time-domain metric.


ISSN: 2591-3522 DOI: 10.70567/mc.v42.ocsid8504

## 1 INTRODUCCIÓN

The present work aims to develop an alternative formulation in the continuous domain to study the dynamic interaction between a moving railway vehicle and the supporting track infrastructure, based on the use of generalized coordinates with global interpolators, which allows efficient coupling of the different parts of the system. This approach offers practical advantages by facilitating the assembly between the discrete models of the vehicle and the foundation with the continuous model of the rail, represented as an Euler-Bernoulli type beam. Moreover, it enables the calculation of the rail's transverse deformation at any point in the continuous domain and at any instant of time, providing a detailed description of its dynamic response.

Among the most important causes of train-induced vibrations are undesired geometric deformations in the wheels, which are originally circular in shape. These deformations, which can appear as localized flat spots (areas with a loss of circularity), alter the ideal rolling condition and cause periodic dynamic excitations in the wheel-rail interaction Zhang et al. (2019b). Several studies have aimed to characterize and quantify the average level of deformation present in wheels during operation. In this regard, the experimental study conducted by (Zhang et al., 2019a) constitutes a significant reference. It is also noteworthy that the irregularities present in the rails contribute significantly to the recorded oscillations. The magnitude and origin of the forces recorded in train wheels have been studied in detail in (Uzzal et al., 2008), as well as the different types of supports that can be modeled between the rail and the foundation ballast (Ferrara et al., 2012).

The model in this work considers the presence of geometric imperfections, both in the wheel and in the longitudinal profile of the rail, which act as sources of unwanted dynamic excitation. As a starting point, an initial approximation is implemented that considers a constant contact stiffness "k", and subsequently, the results are compared with those of an alternative model that considers a direct mass-to-mass type contact, representing a description closer to the system's physical reality.

## 2 MODEL WITH CONSTANT CONTACT STIFFNESS

The dynamic model proposed in this section corresponds to an initial approximation of a locomotive moving over a rail supported by a given structural layer. In this first model the interaction between the locomotive wheels (vehicle) and the rail occurs through a specific contact stiffness (spring element with a specified stiffness). The dynamic model under study is two-dimensional (unknown coordinates: vertical displacements and rotations) and represents half of a freight vehicle. Figure: 1.

### 2.1 Dynamic Equilibrium Equations of the Vehicle

**Dynamic Equilibrium in the Vehicle's Vertical Displacement**

$$\begin{aligned} M_c\,\ddot{y}_c(t) + 2\,C_{s2}\,\dot{y}_c(t) + [-C_{s2}\,l_{lc} + C_{s2}\,l_{rc}]\,\dot{\theta}_c(t) - C_{s2}\,\dot{y}_{b1}(t) - C_{s2}\,\dot{y}_{b2}(t) \\ + 2K_{s2}\,y_c(t) + [-K_{s2}\,l_{lc} + K_{s2}\,l_{rc}]\,\theta_c(t) - K_{s2}\,y_{b1}(t) - K_{s2}\,y_{b2}(t) = -M_c g \end{aligned} \tag{1}$$

**Rotational Dynamic Equilibrium of the Vehicle**

$$\begin{aligned} J_c\,\ddot{\theta}_c(t) + [-C_{s2}\,l_{lc} + C_{s2}\,l_{rc}]\,\dot{y}_c(t) + \left[C_{s2}\,l_{lc}^2 + C_{s2}\,l_{rc}^2\right]\dot{\theta}_c(t) - C_{s2}\,l_{rc}\,\dot{y}_{b1}(t) \\ + C_{s2}\,l_{lc}\,\dot{y}_{b2}(t) + [-K_{s2}\,l_{lc} + K_{s2}\,l_{rc}]\,y_c(t) + \left[K_{s2}\,l_{lc}^2 + K_{s2}\,l_{rc}^2\right]\theta_c(t) \\ - K_{s2}\,l_{rc}\,y_{b1}(t) + K_{s2}\,l_{lc}\,y_{b2}(t) = 0 \end{aligned} \tag{2}$$

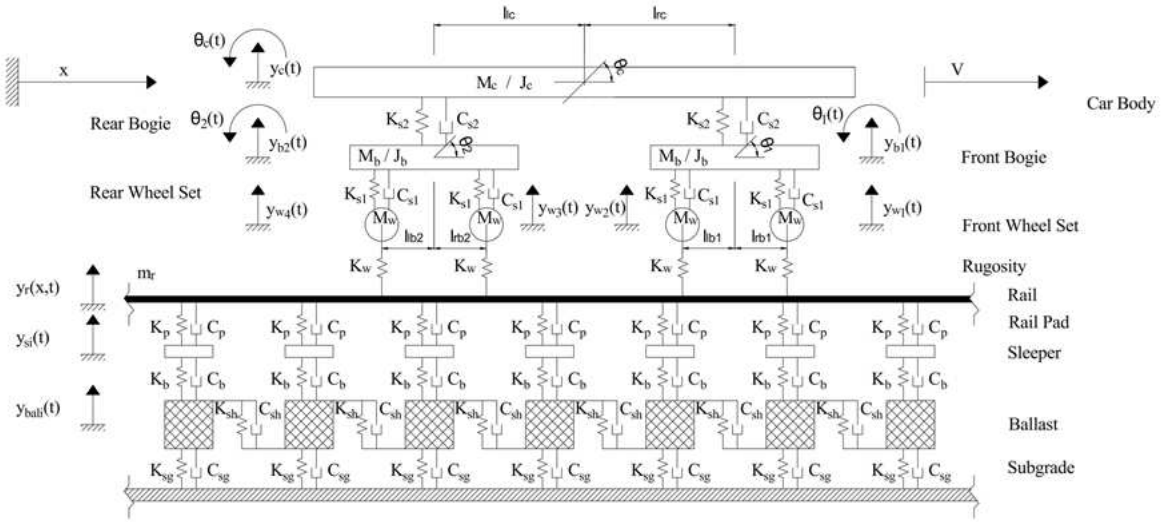


Figure 1: Dynamic model 1

**Dynamic Equilibrium in the Front Bogie's Vertical Displacement**

$$\begin{aligned} M_b\,\ddot{y}_{b1}(t) - C_{s2}\,\dot{y}_c(t) - C_{s2}\,l_{rc}\,\dot{\theta}_c(t) + [C_{s2} + 2C_{s1}]\,\dot{y}_{b1}(t) + [-C_{s1}\,l_{lb1} + C_{s1}\,l_{rb1}]\,\dot{\theta}_1(t) \\ -C_{s1}\,\dot{y}_{w1}(t) - C_{s1}\,\dot{y}_{w2}(t) - K_{s2}\,y_c(t) - K_{s2}\,l_{rc}\,\theta_c(t) + [K_{s2} + 2K_{s1}]\,y_{b1}(t) \\ +[-K_{s1}\,l_{lb1} + K_{s1}\,l_{rb1}]\,\theta_1(t) - K_{s1}\,y_{w1}(t) - K_{s1}\,y_{w2}(t) = -M_{b_1}\,g \end{aligned} \tag{3}$$

**Rotational Dynamic Equilibrium of the Front Bogie**

$$\begin{aligned} J_b\,\ddot{\theta}_1(t) + [-C_{s1}\,l_{lb1} + C_{s1}\,l_{rb1}]\,\dot{y}_{b1}(t) + \left[C_{s1}\,l_{lb1}^2 + C_{s1}\,l_{rb1}^2\right]\,\dot{\theta}_1(t) - C_{s1}\,l_{rb1}\,\dot{y}_{w1}(t) \\ +C_{s1}\,l_{lb1}\,\dot{y}_{w2}(t) + [-K_{s1}\,l_{lb1} + K_{s1}\,l_{rb1}]\,y_{b1}(t) + \left[K_{s1}\,l_{lb1}^2 + K_{s1}\,l_{rb1}^2\right]\,\theta_1(t) \\ -K_{s1}\,l_{rb1}\,y_{w1}(t) + K_{s1}\,l_{lb1}\,y_{w2}(t) = 0 \end{aligned} \tag{4}$$

The same for the Rear Bogie (Vertical displacement and Rotation).

**Dynamic Equilibrium in the Vertical Displacement of Wheel 1**

$$\begin{aligned} M_{w1}\,\ddot{y}_{w1} - C_{s1}\,\dot{y}_{b1}(t) - C_{s1}\,l_{rb1}\,\dot{\theta}_1(t) + C_{s1}\,\dot{y}_{w1}(t) \\ -K_{s1}\,y_{b1}(t) + [K_{s1} + K_w]\,y_{w1}(t) - K_w\,y_{n1_{aux}}(x,t) - K_{s1}\,l_{rb1}\,\theta_1(t) = -M_{w1}\,g \end{aligned} \tag{5}$$

The same for wheels 2, 3 and 4.

**Dynamic Equilibrium Equation for the Vertical Displacement of Node "n aux 1"**

$$-K_w y_{w1}(t) + K_w y_{n1_{aux}}(x,t) = 0 \tag{6}$$

Similarly, the equations for the auxiliary nodes "n" 2 to 4 are obtained correspondingly.

## 2.2 Dynamic Equilibrium Equation for the Vertical Displacement of the Rail Track

The rail for the freight train can be modeled as a continuous Euler-Bernoulli type beam:

$$\rho\,A\,\frac{\partial^2 w(x,t)}{\partial t^2} + E\,I\,\frac{\partial^4 w(x,t)}{\partial x^4} = p(x,t) \tag{7}$$

An approximation is proposed for the rail deformation in the following form:

$$y_r(x,t) = 1 \cdot o(t) + f(x)\,p(t) + \mathcal{B}_{\text{Fourier}}(x) \begin{bmatrix} q_n(t) \\ r_n(t) \end{bmatrix} \tag{8}$$

Where:

$$f(x) = \left[ \frac{x}{l} - \frac{1}{2} + \sum_{p=1}^{k} \frac{1}{p\pi} \sin\left(\frac{2\pi p}{l} x\right) \right] \tag{9}$$

$$\mathcal{B}_{\text{Fourier}}(x) \begin{bmatrix} q_n(t) \\ r_n(t) \end{bmatrix} = \sum_{n=1}^{\infty} \left\{ \sin\left(\frac{2\pi n}{l} x\right) q_n(t) + \cos\left(\frac{2\pi n}{l} x\right) r_n(t) \right\} \tag{10}$$

- The first approximation function is clearly a rigid mode.
- • The second approximation function: $f(x) = \frac{x}{l} - \frac{1}{2} + \sum_{p=1}^{k} \frac{1}{p\pi} \sin\left(\frac{2\pi p}{l} x\right)$ consists of a first part, $\frac{x}{l} - \frac{1}{2}$, which represents a rigid rotation around $x = \frac{l}{2}$, but also includes a set of additional functions, $\sum_{p=1}^{k} \frac{1}{p\pi} \sin\left(\frac{2\pi p}{l} x\right)$, that contribute deformation (curvature). It has been constructed mathematically to be orthogonal to the remaining modes; therefore, it does not capture deformation energy when projected and behaves as a "pseudo-rigid" mode, since it is not a pure rigid mode.

By substituting and expanding, it results in:

$$\begin{aligned} \rho A \left(1\, \ddot{o}(t) + f(x)\, \ddot{p}(t)\right) + \rho A \sum_{n=1}^{k} \left[ \sin\left(\frac{2\pi n}{l} x\right) \ddot{q}_n(t) + \cos\left(\frac{2\pi n}{l} x\right) \ddot{r}_n(t) \right] \\ + E\, I \sum_{n=1}^{k} \frac{1}{n\pi} \left(\frac{2\pi n}{l} x\right)^4 \sin\left(\frac{2\pi n}{l} x\right) p(t) \\ + E\, I \sum_{n=1}^{k} \left(\frac{2\pi n}{l}\right)^4 \left[ \sin\left(\frac{2\pi n}{l} x\right) q_n(t) + \cos\left(\frac{2\pi n}{l} x\right) r_n(t) \right] = p(x,t) \end{aligned} \tag{11}$$

By applying the Weighted Residuals method (Galerkin Method), the previous system is projected onto the different weighting functions used to interpolate the beam. Thus, both sides are multiplied by the following weighting functions:

$$w_i(x) = \left\{ 1,\ f(x),\ \sin\left(\frac{2\pi p}{l} x\right),\ \cos\left(\frac{2\pi p}{l} x\right) \ \middle|\ p = 1, 2, 3, \ldots, k \right\} \tag{12}$$

Which yields:

$$\rho\, A\, l\, \ddot{o}(t) = \int_0^l p\,(x,t)\ w_1\,(x)\ dx \tag{13}$$

$$\rho\, A\, l\, \ddot{p}(t) = \int_0^l p(x,t)\ w_2(x)\ dx \tag{14}$$

$$\rho\, A\, \frac{l}{2}\, \ddot{q}_p(t) + E\, I\, \frac{l}{2}\, \frac{1}{p\,\pi} \left(\frac{2\pi p}{l}\right)^4 p(t) + E\, I\, \frac{l}{2} \left(\frac{2\pi p}{l}\right)^4 q_p(t) = \int_0^l p(x,t)\, w_3(x)\, dx \tag{15}$$

$$\rho\, A\, \frac{l}{2}\, \ddot{r}_p(t) + E\, I\, \frac{l}{2} \left(\frac{2\pi p}{l}\right)^4 r_p(t) = \int_0^l p(x,t)\, w_4(x)\, dx \tag{16}$$

For values of $p = 1, 2, 3, \ldots, k$, where $k$ is the number of interpolation degrees (for the trigonometric functions) chosen to be used.

### 2.3 Dynamic Equilibrium Equation for the Vertical Displacement of Node "nn aux, I-th"

$$C_p\,\dot{y}_{nn\,i\text{-th}_{aux}}(t) - C_p\,\dot{y}_{s\,i\text{-th}_{aux}}(x,t) + K_p\,y_{nn\,i\text{-th}_{aux}}(t) - K_p\,y_{s\,i\text{-th}_{aux}}(x,t) = 0 \tag{17}$$

**Dynamic Equilibrium Equation for the Vertical Displacement of the Sleepers**

$$\begin{aligned} M_{s_i}\,\ddot{y}_{s_i} + [C_p + C_b]\;\dot{y}_{s_i}(t) - C_b\,\dot{y}_{b_i}(t) - C_p\,\dot{y}_{nn_{i_{aux}}}(t) \\ + [K_p + K_b]\;y_{s_i}(t) - K_b\,y_{b_i}(t) - K_p\,y_{nn_{i_{aux}}}(t) = -M_{s_i}g \end{aligned} \tag{18}$$

**Dynamic Equilibrium Equation for the Vertical Displacement of the Ballast**

$$\begin{aligned} M_{b_i}\,\ddot{y}_{b_i} - C_b\,\dot{y}_{s_i}(t) - C_{sh}\,\dot{y}_{b_{i-1}}(t) + [C_b + C_{sg} + 2C_{sh}]\;\dot{y}_{b_i}(t) - C_{sh}\,\dot{y}_{b_{i+1}}(t) - K_b\,y_{s_i}(t) \\ -K_{sh}\,y_{b_{i-1}}(t) + [K_b + K_{sg} + 2K_{sh}]\;y_{b_i}(t) - K_{sh}\,y_{b_{i+1}}(t) = -M_{b_i}g \end{aligned} \tag{19}$$

With $i = 1, 2, 3, \ldots, N$, where $N$ is the total number of sleepers/ballasts considered in the model.

### 2.4 Matrix Assembly of the Dynamic Equilibrium Equation System for Dynamic Interaction Model No. 1

$$[M] = \begin{bmatrix} [M_{\text{vehicle}}] & [0] & [0] \\ [0] & [M_{\text{rail}}] & [0] \\ [0] & [0] & [M_{\text{foundation}}] \end{bmatrix} \tag{20}$$

$$[C] = \begin{bmatrix} [C_{\text{vehicle}}] & [0] & [0] \\ [0] & [0] & [0] \\ [0] & [0] & [C_{\text{foundation}}] \end{bmatrix} \tag{21}$$

$$[K] = \begin{bmatrix} [K_{\text{vehicle}}] & [0] & [0] \\ [0] & [K_{\text{rail}}] & [0] \\ [0] & [0] & [K_{\text{foundation}}] \end{bmatrix} \tag{22}$$

### 2.5 Reduction of Degrees of Freedom

By working with auxiliary nodes, it is possible to establish a relationship that links them to the primary coordinates of the model, thus reducing the number of unknowns and simultaneously coupling the system across its different components. For the nodes connecting the vehicle to the rail, assuming that their displacements must be identical, a generic expression can be formulated as:

$$y_{n_{aux}}(x,t) = y_r(x,t) \tag{23}$$

Similarly, for the nodes connecting the rail to the sleepers, with $x_j = x_{\text{sleepers}}$:

The reduction of the system of equations, by eliminating the "auxiliary nodes", can be

schematically represented through the following coordinate transformation:

$$\begin{bmatrix} y-\theta_{\text{vehiculo}}(t) \\ y_{ni_{\text{aux}}}(t) \\ z_i(t) \\ y_{nni_{\text{aux}}}(t) \\ y_{s_i}(t) \\ y_{b_i}(t) \end{bmatrix} = \overbrace{\begin{bmatrix} I_{10\times 10} & 0 & 0 & 0 \\ 0 & Y_n(x_w) & 0 & 0 \\ 0 & I_{k\times k} & 0 & 0 \\ 0 & Y_n(x_i) & 0 & 0 \\ 0 & 0 & I_{N\times N} & 0 \\ 0 & 0 & 0 & I_{N\times N} \end{bmatrix}}^{[L]} \begin{bmatrix} y-\theta_{\text{vehiculo}}(t) \\ z_i(t) \\ y_{s_i}(t) \\ y_{b_i}(t) \end{bmatrix} \tag{24}$$

With:

$$\begin{aligned} \{y\} &= [L]\{y_{\text{reduced}}\} \\ \{\dot{y}\} &= [L]\{\dot{y}_{\text{reduced}}\} \\ \{\ddot{y}\} &= [L]\{\ddot{y}_{\text{reduced}}\} \end{aligned} \tag{25}$$

Yielding:

$$\begin{aligned} [M]\{\ddot{y}\} + [C]\{\dot{y}\} + [K]\{y\} &= [f] \\ [L]^T[M][L]\{\ddot{y}_{\text{reduced}}\} + [L]^T[C][L]\{\dot{y}_{\text{reduced}}\} + [L]^T[K][L]\{y_{\text{reduced}}\} &= [L]^T[f] \end{aligned} \tag{26}$$

This defines the system of dynamic equilibrium equations to be solved. The following matrices are defined:

$$\begin{aligned} [M_{\text{reduced}}] &= [L]^T[M][L] \\ [C_{\text{reduced}}] &= [L]^T[C][L] \\ [K_{\text{reduced}}] &= [L]^T[K][L] \\ [f_{\text{reduced}}] &= [L]^T[f] \end{aligned} \tag{27}$$

Expressing the system in state-space form:

$$\begin{aligned} \begin{bmatrix} \dot{y}_{\text{red}} \\ \ddot{y}_{\text{red}} \end{bmatrix} &= \begin{bmatrix} \dot{y}_{\text{red}} \\ \left([L]^T[M][L]\right)^{-1} \left\{ -[L]^T[C][L]\{\dot{y}_{\text{reduced}}\} - [L]^T[K][L]\{y_{\text{reduced}}\} + [L]^T\{f\} \right\} \end{bmatrix} \\ \begin{bmatrix} \dot{y}_{\text{red}} \\ \ddot{y}_{\text{red}} \end{bmatrix} &= \begin{bmatrix} 0 & I \\ -M_{\text{red}}^{-1}K_{\text{red}} & -M_{\text{red}}^{-1}C_{\text{red}} \end{bmatrix} \begin{bmatrix} y_{\text{red}} \\ \dot{y}_{\text{red}} \end{bmatrix} + \begin{bmatrix} 0 \\ M_{\text{red}}^{-1}f_{\text{red}} \end{bmatrix} \\ \dot{x} &= Ax + B \end{aligned} \tag{28}$$

### 2.6 Model parameters and simulation cases

Model parameters are defined in Table 1. First, a case at very low speed is run to verify the formulation. Secondly, some simulation results of dynamic deflections due to rail roughness and wheel deformation are presented.

### 2.7 Results: Comparison between Static and Dynamic Deflections (low speed)

The dynamic deflections of the beam (rail) are determined for the vehicle moving at a reduced speed ($V = 1\,\frac{km}{h}$ — quasi-static behavior). The results obtained are compared with the

Table 1: Parameters used in the dynamic train model

| Parameter | Symbol | Value | Unit |
|---|---|---|---|
| Vehicle displacement speed | $V$ | 36 | $\mathrm{km/h}$ |
| Half of locomotive mass | $M_c$ | 38,800 | $\mathrm{kg}$ |
| Locomotive moment of inertia | $J_c$ | 1,564.933 | $\mathrm{kg\,m^2}$ |
| Distance CM locomotive to front bogie CM | $l_{rc}$ | 11.875 | $\mathrm{m}$ |
| Distance CM locomotive to rear bogie CM | $l_{lc}$ | 11.875 | $\mathrm{m}$ |
| Secondary suspension stiffness | $K_{s2}$ | 6.11 | $\mathrm{MN/m}$ |
| Secondary suspension damping | $C_{s2}$ | 90 | $\mathrm{kN\,s/m}$ |
| Half of bogie mass | $M_b$ | 1500 | $\mathrm{kg}$ |
| Distance CM front bogie to right wheel | $l_{b1r}$ | 0.625 | $\mathrm{m}$ |
| Distance CM front bogie to left wheel | $l_{b1l}$ | 0.625 | $\mathrm{m}$ |
| Bogie moment of inertia | $J_b$ | 176 | $\mathrm{kg\,m^2}$ |
| Primary suspension stiffness | $K_{s1}$ | 7.88 | $\mathrm{MN/m}$ |
| Primary suspension damping | $C_{s1}$ | 52.5 | $\mathrm{kN\,s/m}$ |
| Wheel mass | $M_w$ | 500 | $\mathrm{kg}$ |
| Wheel radius | $R$ | 0.42 | $\mathrm{m}$ |
| Wheel-rail contact stiffness | $K_w$ | $5\,K_{s1}$ | $\mathrm{MN/m}$ |
| Rail linear mass | $m_r$ | 60.64 | $\mathrm{kg/m}$ |
| Rail flexural stiffness | $EI$ | 6.62 | $\mathrm{MN\,m^2}$ |
| Rail cross-section area | $A_r$ | 0.00767 | $\mathrm{m^2}$ |
| Rail material density | $\rho$ | 7900 | $\mathrm{kg/m^3}$ |
| Rail length | $l$ | 90 | $\mathrm{m}$ |
| Rail pad stiffness | $K_p$ | 120 | $\mathrm{MN/m}$ |
| Rail pad damping | $C_p$ | 75 | $\mathrm{kN\,s/m}$ |
| Half sleeper mass | $M_s$ | 118.5 | $\mathrm{kg}$ |
| Sleeper spacing | $l_s$ | 0.6 | $\mathrm{m}$ |
| Ballast stiffness | $K_b$ | 182 | $\mathrm{MN/m}$ |
| Ballast damping | $C_b$ | 58.8 | $\mathrm{kN\,s/m}$ |
| Half ballast mass | $M_b$ | 739 | $\mathrm{kg}$ |
| Sub-base stiffness | $K_{sg}$ | 78.4 | $\mathrm{MN/m}$ |
| Sub-base damping | $C_{sg}$ | 31.15 | $\mathrm{kN\,s/m}$ |
| Ballast shear stiffness | $K_{sh}$ | 147 | $\mathrm{MN/m}$ |
| Ballast shear damping | $C_{sh}$ | 80 | $\mathrm{kN\,s/m}$ |
| Initial position | $x_0$ | 25 | $\mathrm{m}$ |
| Number of interpolation functions for rail | $n$ | 10 | – |

static deformations of the rail for the same vehicle at rest ($V = 0\,\frac{km}{h}$), positioned at different locations ($x_{w1}$) along the length of the domain. In the figure below, it can be observed one of the results obtained. The correspondence between both deflections is absolute in each of the cases that were analyzed. Figure: 2.

## 3 DYNAMIC INTERACTION MODEL WITH DIRECT MASS-TO-MASS CONTACT

Considering, in a general form, that:

$$y(t) = L(t)\, y_{\text{red}}(t) \tag{29}$$

with $y(t) \in \mathbb{R}^n$ and $L(t) \in \mathbb{R}^{n\times m}$ with $m < n$, and therefore $y_{\text{red}}(t) \in \mathbb{R}^m$, the system possesses **kinetic energy**, **potential energy**, and **dissipative forces** (i.e., it is a **non-conservative**

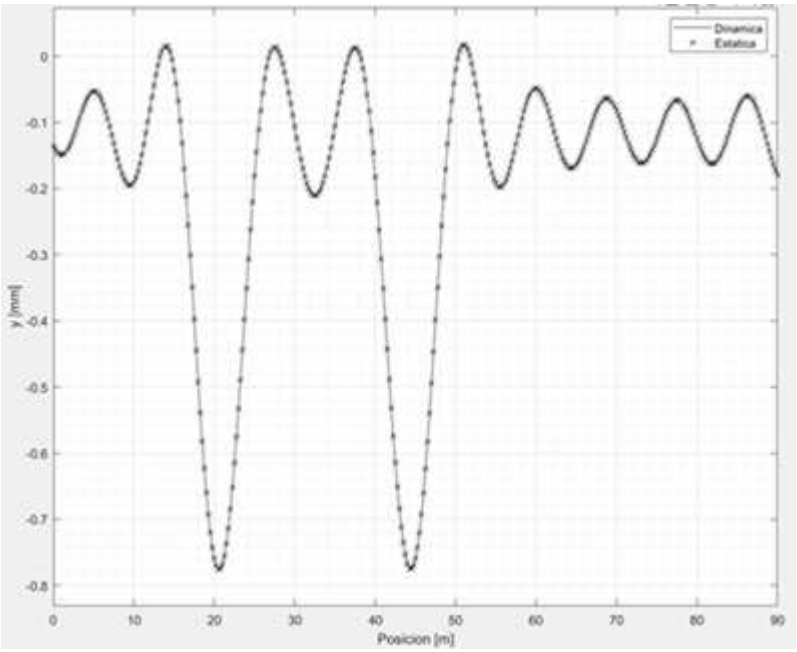


Figure 2: Comparison: Static vs. Dynamic Rail Deformation

**system**).

**Kinetic Energy**

$$T = \frac{1}{2}\dot{y}^T M \dot{y} \tag{30}$$

Taking into account that:

$$\begin{aligned} \dot{y} &= \frac{d}{dt}\big(y(t)\big) \\ &= \dot{L}\, y_{\text{red}} + L\, \dot{y}_{\text{red}} \end{aligned} \tag{31}$$

Results:

$$T = \frac{1}{2}\, y_{\text{red}}^T\, \dot{L}^T M\, \dot{L}\, y_{\text{red}} + \dot{y}_{\text{red}}^T L^T M\, \dot{L}\, y_{\text{red}} + \frac{1}{2}\, \dot{y}_{\text{red}}^T L^T M L\, \dot{y}_{\text{red}}$$

**Potential Energy**

$$V = \frac{1}{2}\, y_{\text{red}}^T\, L^T\, K\, L\, y_{\text{red}} \tag{32}$$

**Lagrangian**

$$\mathcal{L} = T - V \tag{33}$$

**Non-conservative force term** For the reduced generalized coordinates $y_{\text{red}}$, the generalized forces are:

$$Q_{\text{red}} = L^T \Big( f - C\, (\dot{L}\, y_{\text{red}} + L\, \dot{y}_{\text{red}}) \Big) \tag{34}$$

**Equations of Motion**

$$\frac{d}{dt}\left(\frac{\partial \mathcal{L}}{\partial \dot{y}_{\text{red}}}\right) - \frac{\partial \mathcal{L}}{\partial y_{\text{red}}} = Q_{\text{red}} \tag{35}$$

Defining:

$$M_{\text{red}}(t) = L^T M L \tag{36}$$

$$B(t) = L^T M \dot{L} \tag{37}$$

$$K_{\text{red}}(t) = L^T K L \tag{38}$$

The Lagrangian becomes:

$$\mathcal{L} = \frac{1}{2} y_{\text{red}}^T \dot{L}^T M \dot{L} y_{\text{red}} + \dot{y}_{\text{red}}^T L^T M \dot{L} y_{\text{red}} + \frac{1}{2} \dot{y}_{\text{red}}^T M_{\text{red}} \dot{y}_{\text{red}} - \frac{1}{2} y_{\text{red}}^T K_{\text{red}} y_{\text{red}} \tag{39}$$

$$\mathcal{L} = T - V \tag{40}$$

By differentiating with respect to time and manipulating (35), one obtains:

$$M_{\text{red}}(t)\, \ddot{y}_{\text{red}} + C_{\text{resultante}}(t)\, \dot{y}_{\text{red}} + K_{\text{resultante}}(t)\, y_{\text{red}} = f_{\text{red}} \tag{41}$$

where:

$$\begin{aligned}
M_{\text{red}}(t) &= L^T\, M\, L \\
\\
C_{\text{resultante}}(t) &= \dot{M}_{\text{red}}(t) + B(t) - B^T(t) + F(t) \\
\dot{M}_{\text{red}}(t) &= \dot{L}^T\, M\, L + L^T\, M\, \dot{L} \\
&= \dot{L}^T\, M\, L + B(t) \\
B(t) &= L^T\, M\, \dot{L} \\
F(t) &= L^T\, C\, L \\
\\
K_{\text{resultante}}(t) &= \dot{B}(t) - D(t) + K_{\text{red}}(t) + E(t) \\
D(t) &= \dot{L}^T\, M\, \dot{L} \\
\dot{B}(t) &= \dot{L}^T\, M\, \dot{L} + L^T\, M\, \ddot{L} \\
&= D(t) + L^T\, M\, \ddot{L} \\
K_{\text{red}}(t) &= L^T\, K\, L \\
E(t) &= L^T\, C\, \dot{L} \\
\\
f_{\text{red}} &= L^T\, f
\end{aligned} \tag{42}$$

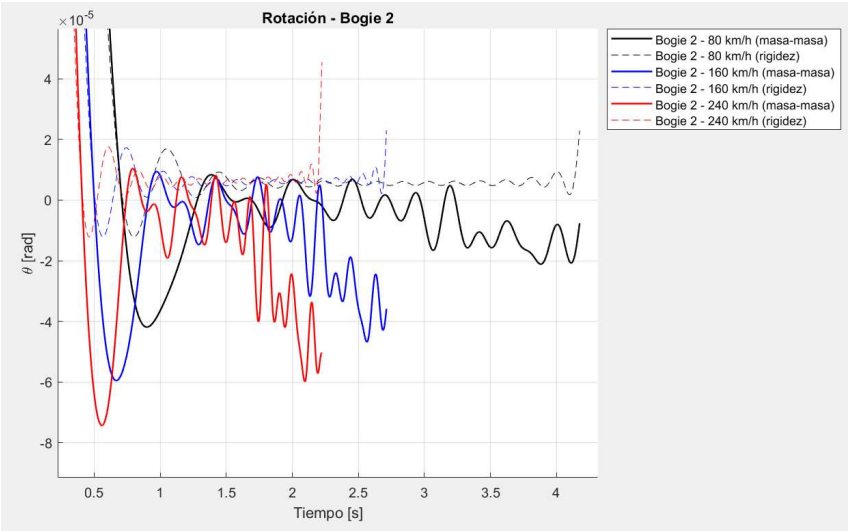


Figure 3: Rotation Bogie 2. Rigid and Contact mass-to-mass model comparison

## 4 CONCLUSIONS

The computed response is consistent with the physical phenomenon intended to be represented, which validates the approach used for analyzing the system without and with track irregularities.

The simplified model that incorporates contact stiffness using a sufficiently high value of $k$ (to simulate a rigid interface, e.g., $k = 5\,K_{s1}$), shows significant advantages compared to the full model (contact mas-to-mass). The structural simplicity of the reduced model facilitates its implementation and assembly, making it particularly suitable for exploratory simulations (the contact-stiffness model can reduce simulation time by up to 90% compared to the mass-to-mass contact model).

The dynamic results obtained from both models are similar. It is observed that the mass-to-mass contact model exhibits a slightly higher frequency content in the vehicle degrees of freedom (DOFs) compared to the flexible-contact model (model with $k$). The latter, being structurally more flexible, allows slightly larger displacements, although without compromising simulation fidelity. The full model reflects a more accurate representation of the oscillations occurring at the vehicle level (these show slightly higher values when the train speed exceeds 200 $\frac{\text{km}}{\text{h}}$). Both models accurately simulate rail deflections, showing negligible numerical differences in this regard. Figure: 3.

## REFERENCES

Ferrara R., Leonardi G., and Jourdan F. Numerical modelling of train induced vibrations. *Procedia-Social and Behavioral Sciences*, 53:155–165, 2012.

Uzzal R.U.A., Ahmed W., and Rakheja S. Dynamic analysis of railway vehicle-track interactions due to wheel flat with a pitch-plane vehicle model. *Journal of Mechanical Engineering*, 39(2):86–94, 2008.

Zhang H., Ren Z., Wu Q., and Yang J. Simulation on metro railway induced vibration. part ii: effect of corrugated rail. *Vibroengineering Procedia*, 29:136–140, 2019a.

Zhang H., Ren Z., Zhang H., and Liu Q. Simulation on metro railway induced vibration. part i: effect of out-of-round wheels. *Vibroengineering Procedia*, 29:130–135, 2019b.